Methanol oxidation on carbon-supported platinum–tin electrodes in sulfuric acid

A.S. Aricò, V. Antonucci and N. Giordano
CNR Institute for Transformation and Storage of Energy, Santa S. Lucia Sopra Contesse 39, 98126 S. Lucia, Messina (Italy)

A.K. Shukla*, M.K. Ravikumar, A. Roy, S.R. Barman and D.D. Sarma
Solid State and Structural Chemistry Unit, Indian Institute of Science, Bangalore 560 012 (India)

(Received September 13, 1993; accepted January 13, 1994)

Abstract

A study is made of the electrooxidation of methanol in sulfuric acid on carbon-supported electrodes containing platinum–tin bimetal catalysts that are prepared by an *in situ* potentiometric-characterization route. The catalysts are investigated by employing chemical analyses, X-ray diffraction (XRD), X-ray absorption-near-edge spectroscopy (XANES) and X-ray photoelectron spectroscopy (XPS) data in conjunction with electrochemical measurements. From the electrochemical data, it is inferred that while an electrode with (3:1) Pt–Sn/C catalyst involves a two-electron rate-limiting step akin to platinum-on-carbon electrodes, it is shifted to a one-electron mechanism on electrodes with (3:2)Pt–Sn/C, (3:3)Pt–Sn/C, and (3:4)Pt–Sn/C catalysts. The study suggests that the tin content in the platinum–tin bimetal catalyst produces: (i) a charge transfer from tin to platinum; (ii) an increase in the coverage of adsorbed methanolic residues with increase in the tin content, as indicated by the shift in rest potential of the electrodes towards the reversible value for oxidation of methanol (0.043 V versus SHE), and (iii) a decrease in the overall content of higher valent platinum sites in the catalyst.

Introduction

Chemists are challenged by the desire to use a liquid fuel in a fuel cell, as fuel is best transported and converted into energy from the liquid state. Methanol is the favoured fuel [1–5]. The direct methanol/air fuel cell (DMFC) uses a sulfuric acid electrolyte because of the need to reject the CO_2 that is produced during the electrooxidation of methanol. It is also imperative to employ a catalyst that is platinum–metal based. Nevertheless, a major scientific problem is the catalyst poisoning caused by residues of an aldehyde, carboxylic acid and other intermediates that are produced during the electrooxidation of methanol [6–14].

The electrocatalytic activity of the platinum catalyst is known to be promoted in the presence of a second metal, such as ruthenium or tin, that configures as an adatom or a bimetal. The process by which such a synergistic promotion of the methanol-oxidation reaction is brought about by these catalysts has been a subject of study during the last few years. In these investigations, spectroscopic methods have been employed in conjunction with electrochemical techniques [15–33]. Although the syn-

*Author to whom correspondence should be addressed.

SSDI 0378-7753(94)01908-E

ergistic activity of Pt–Ru catalysts towards the methanol-oxidation reaction has been established, the behaviour of Pt–Sn catalysts has still to be determined. This is particularly so for electrodes of fuel cell configurations that require the catalyst to be supported on an active carbon and, thereby, impose an altogether different morphological situation in relation to the bulk-metal catalyst.

This study reports some spectroscopic investigations that were conducted in conjunction with electrochemical experiments in an attempt to understand the role of tin in Pt–Sn bimetal catalysts of varying compositions. These catalysts are dispersed on a high-surface-area carbon support in order to mimic the conditions of fuel cell electrodes.

Experimental

Preparation and characterization of carbon-supported catalysts

In the preparation of Pt–Sn/C catalysts, 5 g of Ketjen black-EC carbon was suspended in 300 cm^3 of water and agitated in an ultrasonic bath with constant stirring at 80 °C. Appropriate volumes of the solutions of chloroplatinic acid in water and tin chloride in dilute HCl were slowly added to the carbon suspension under constant stirring with the temperature still maintained at about 80 °C. The resulting mass was left for 1 h with constant stirring in order to achieve complete impregnation of the carbon with the chloroplatinic acid and tin chloride solutions. This was followed by drop-wise addition of 0.2 M hydrazine solution to a level that was slightly higher than the stoichiometric amount required for complete reduction to platinum and tin metals. Subsequently, 0.5 M NaOH solution was added to the slurry to bring the pH to near neutral. The mixture was filtered, washed copiously with hot distilled water, and then dried in an air oven at 110 °C.

Preparation of Pt/C and Sn/C catalysts

The carbon-supported platinum catalyst (16.6 wt.%) was prepared by reduction of chloroplatinic acid following a procedure similar to that used for the Pt–Sn/C catalysts. A specimen of carbon-supported tin (7.2 wt.%) was also obtained from tin chloride solution in dilute hydrochloric acid in a similar fashion.

Potentiometric and spectroscopic characterization

The variations in potential during the preparation of Sn/C, Pt/C, (3:1)Pt–Sn/C, (3:2)Pt–Sn/C, (3:3)Pt–Sn/C, and (3:4)Pt–Sn/C were recorded *in situ* using a spiral platinum electrode versus a saturated calomel electrode (SCE); the concomitant changes in pH were monitored with a temperature-compensated pH probe. Absorption spectra of the solutions containing catalyst precursors and their filtrates after reduction of the catalysts were recorded in the ultraviolet and visible regions of a U-3410 Hitachi spectrometer. The quantitative elemental analyses of various catalysts were carried out on an automatic EA1108-Carlo Erba elemental analyser.

Characterization of catalysts by X-ray diffraction (XRD), X-ray absorption-near-edge spectroscopy (XANES) and X-ray photoelectron spectroscopy (XPS)

XRD patterns of Pt/C, (3:1)Pt–Sn/C, (3:2)Pt–Sn/C, (3:3)Pt–Sn/C, (3:4)Pt–Sn/C and Sn/C, after treatment of each catalyst in air at 350 °C for 15 min, were recorded at room temperature on a Stoe X-ray diffractometer using a Cu Kα radiation source. The (3:1)Pt–Sn/C, (3:2)Pt–Sn/C, (3:3)Pt–Sn/C, (3:4)Pt–Sn/C and Sn/C samples were

also heated in vacuum at 400 °C for about 2 h, in order to attain better crystallinity of the component phases; the XRD patterns were then obtained.

The XANES data on samples Pt/C, (3:2)Pt–Sn/C and (3:4)Pt–Sn/C (after treatment in air at 350 °C for 15 min) were obtained by recording the Pt(L_{III}) X-ray absorption edges with a Rigaku X-ray absorption spectrometer coupled to a Ru-200B Rigaku rotating anode X-ray generator. The monochromator employed was a Si(440) crystal with a 0.1 mm slit.

XPS of Pt/C and (3:2)Pt–Sn/C samples, again after treatment of the catalysts in air at 350 °C for 15 min, were recorded at 30 °C on an XPS–UPS–BIS spectrometer that employed Mg Kα radiation. The vacuum in the analysis chamber of the instrument was better than 10^{-9} torr. The recorded spectra were analysed in terms of two or three different species of platinum. As the spectral shapes of the various components are not known a priori, it was assumed that, except for a possible variation in the spectral widths, the line shapes of the different components of the platinum species were the same for carrying out the spectral decompositions. For this purpose, it was elected to use XPS data for platinum metal taken from the literature [34]. The widths of the components were allowed to change by convoluting Gaussian distributions of different widths with the platinum spectrum given in ref. 34. The Gaussian broadening is supposed to account for differences in the instrumental resolution, phonon broadening, and other effects. The spectral decompositions were carried out with a least-square-error procedure by varying the Gausssian widths, energy positions, and the intensities of the components. All reported binding energies of the platinum 4f level are for platinum $4f_{7/2}$; the spin-orbit splitting is 3.2 eV for all components.

Electrode preparation and characterization

Electrodes with various Pt–Sn/C and Pt/C catalysts were prepared by first mixing the catalyst with water at 60 °C in an ultrasonic bath with constant mechanical stirring for about 30 min. Subsequently, a 10 wt.% suspension of Teflon was slowly added with constant stirring over a period of 30 min. An appropriate amount of isopropyl alcohol was then introduced and the slurry was allowed to stand for 2 h. The resulting paste was spread over Toray carbon paper that was treated with tetrafluoroethylene–hexafluoropropylene copolymer dispersion (FEP) (5 mg cm^{-2}) and hot pressed at 70 °C under 15 kg cm^{-2} pressure for a period of 5 min. The electrodes were first dried in an air oven at 110 °C for about 1 h and then treated in air at 350 °C for 15 min in the same oven. The platinum loading in all the electrodes was 0.8 mg cm^{-2}.

Galvanostatic current–potential measurements for the oxidation of methanol (1 M) in sulfuric acid (2.5 M) were conducted on Pt–Sn/C and Pt/C electrodes at 60 °C in a three-electrode, jacketed cell. The test regime was applied with a Tacussel model PJT 24-1 galvanostat/potentiostat. The working electrode was mounted on a perforated platinum-foil current-collector in a Teflon holder. The latter had provision for CO_2 evolved during the electrode polarization to escape from its rear. A SCE was employed for polarization measurements; the Luggin tip was placed appropriately close to the working electrode [35]. The polarization data are reported, however, with respect to the standard hydrogen electrode (SHE). The electrolyte was flushed with nitrogen and stirred throughout the measurements. Ohmic-drop measurements on various electrodes were performed with a Philips storage oscilloscope (model PM3375) that was coupled to a fast on/off switching circuit.

Results and discussion

The concomitant changes in potential and pH with volume of the impregnating solution during impregnation of the carbon support with platinum, as well as for some typical compositions of Pt–Sn bimetals are shown in Fig. 1. The carbon employed in this study has a pH-of-zero-zeta potential (pzzp) value of 9.85 and, as expected, bears a positive charge at lower pH. Supposedly, this charge facilitates the electrostatic interaction between the carbon surface and the $[PtCl_6]^{2-}$ precursor [36]. The potential increases sharply during impregnation of the carbon with platinum and Pt–Sn precursors and settles at values between 400 to 600 mV versus SCE, as determined by the catalyst composition. The observed potential for impregnation of the Pt/C catalyst is close to the redox potential for the Pt^{4+}/Pt^0 couple, but decreases progressively for the other catalysts as the Sn^{2+} content is increased in the solution. It is noteworthy that a potential of -160 mV versus SCE has been observed after impregnation of carbon with a similar amount of $SnCl_2$ in dilute HCl.

UV-visible absorption spectra for an impregnating solution of (3:4)Pt–Sn catalyst precursor at various dilutions are shown in Fig. 2(a). Evidence for the formation of a $[PtCl_2(SnCl_3)_2]^{2-}$ complex is provided by the typical absorption band at 278 nm that

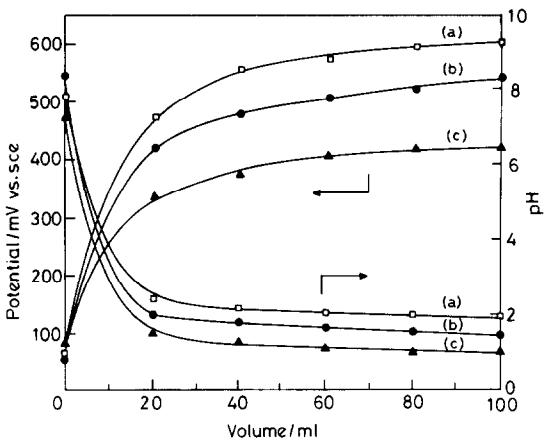

Fig. 1. Variation in potential and pH with volume of impregnating solution during impregnation of the carbon-black supports with the Pt–Sn precursor for (a) Pt/C; (b) (3:2)Pt–Sn/C, and (c) (3:4)Pt–Sn/C catalysts.

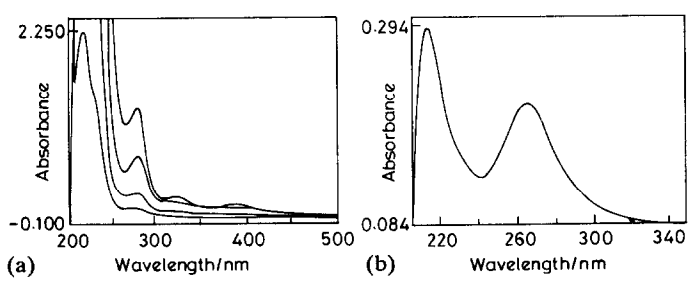

Fig. 2. UV-visible absorption spectra of impregnating solutions containing precursors of (a) (3:4)Pt–Sn/C, and (b) (3:2)Pt–Sn/C catalysts.

is due to charge transfer from $(SnCl_3)^{2-}$ to Pt^{2+} [37]. The absorption bands observed for this precursor at 385 and 320 nm are most likely from the same complex and could arise from d–d transitions within the platinum sites [37]. By contrast, no evidence for the presence of a $(PtCl_6)^{2-}$ complex in this solution is found from the spectra. The absorption band at 214 nm is attributed to an Sn^{4+} species. The complex $(PtCl_4)^{2-}$ [37, 38] cannot be detected because of its low absorption coefficient. The $[PtCl_2(SnCl_3)_2]^{2-}$ complex is not found to be present in the impregnating solution of (3:2)Pt–Sn precursor (Fig. 2(b)) as only the absorption bands typical of $(PtCl_6)^{2-}$ and Sn^{4+} at 262 and 210 nm [37], respectively, are detectable.

During the reduction of the Pt–Sn precursor by hydrazine, the potential is found to decrease progressively with a concomitant decrease in pH due to production of HCl following the reaction:

$$H_2PtCl_6 + 4e^- \longrightarrow Pt^0 + 2HCl + 4Cl^- \quad (1)$$

The changes in potential and pH during the reduction of catalyst precursors to Pt/C, (3:2)Pt–Sn/C and (3:4)Pt–Sn/C catalysts are given in Figs. 3 and 4. The variations in pH cease on adding 5 mM of hydrazine; this indicates complete reduction to platinum (Fig. 3). The potentiometric data in Fig. 4 show that the amount of hydrazine required for the reduction of (3:2)Pt–Sn/C and (3:4)Pt–Sn/C catalysts is about 5 and 3 mM, respectively. The dilution of solution on further addition of hydrazine in both (3:2)Pt–Sn/C and (3:4)Pt–Sn/C catalyst precursors pushes up the pH, while the potential settles at about -100 mV versus SCE. The inflection point observed in the potentiometric curve for (3:2)Pt–Sn/C preparation is indicative of a reduction process that proceeds in two steps, namely: $Pt^{4+} \rightarrow Pt^{2+}$, followed by $Pt^{2+} \rightarrow Pt^0$. This is also observed in the data for the Pt/C catalyst given in Fig. 3. The neutralization of solutions with NaOH drives the potential to about -600 mV versus SCE in the Pt–Sn catalysts and, therefore, shifts the equilibrium to $Sn^{2+} \rightarrow Sn$ [39]. A typical plot for a (3:2)Pt–Sn/C catalyst that displays this behaviour is presented in Fig. 5.

The XRD patterns for various specimens of Pt–Sn/C catalyst treated in air at 350 °C for 15 min and for those vacuum treated at 400 °C for about 2 h are given in Figs. 6(a) and (b), respectively. For the (3:4)Pt–Sn/C catalysts the data show the formation of a single Pt–Sn alloy phase, along with Pt and SnO_2. In other Pt–Sn/C

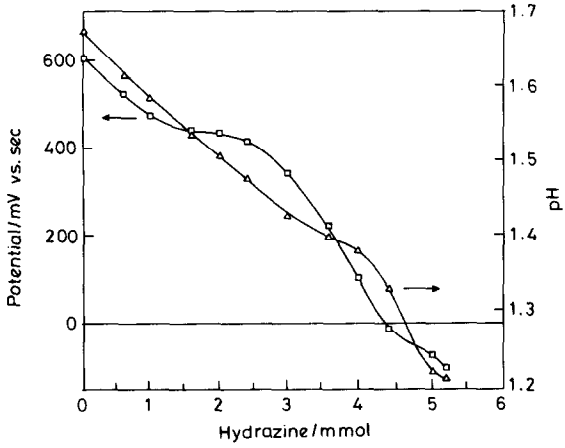

Fig. 3. Variation in potential and pH during reduction process of Pt/C catalyst.

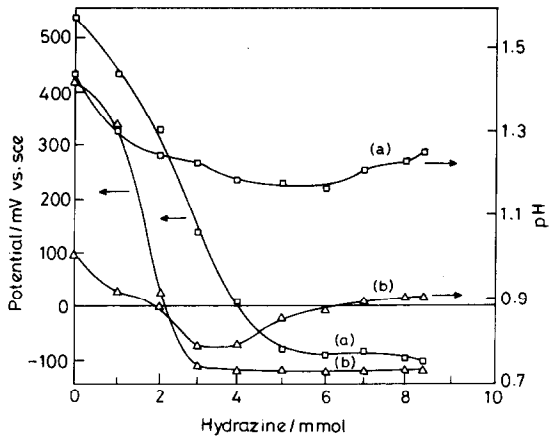

Fig. 4. Variation in potential and pH during reduction process in preparation of (a) (3:2)Pt–Sn/C, and (b) (3:4)Pt–Sn/C catalysts.

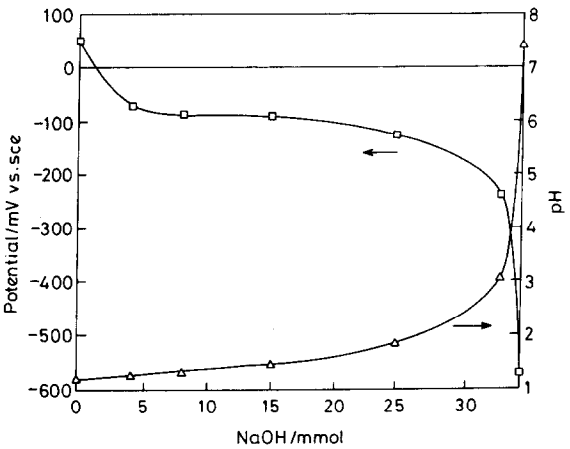

Fig. 5. Variation in potential and pH during neutralization process in preparation of (3:2)Pt–Sn/C catalyst.

samples (namely: (3:1)Pt–Sn/C, (3:2)Pt–Sn/C and (3:3)Pt–Sn/C)), however, the admixtures of Pt_3Sn and Pt–Sn alloy phases are found to be present, along with Pt and SnO_2 [40]. This signifies that for the formation of the Pt–Sn alloy, it is mandatory to have proportionally higher contents of tin in the impregnating solutions. Chemical analyses of various catalyst samples given in Table 1 indeed indicate the higher tin content in (3:4)Pt–Sn/C. It is noteworthy that the diffraction peaks seen at 2θ values close to 80° are common to all the Pt–Sn/C catalyst samples and are characteristic of platinum and Pt–Sn alloy phases [26]. The average size of the catalyst particles in Pt/C, Pt–Sn/C catalysts prior to the heat treatment — as obtained from the broadening of XRD peaks and the Debye–Scherrer equation [41] — is found to be ~100 Å.

The XANES data show that the maximum in the peak corresponding to the $2p_{3/2} \rightarrow 5d$ transition in the Pt/C carbon sample occurs at 11.551 keV (Fig. 7(a)). The peak is shifted to lower energy values both for the (3:2)Pt–Sn/C (Fig. 7(b)) and

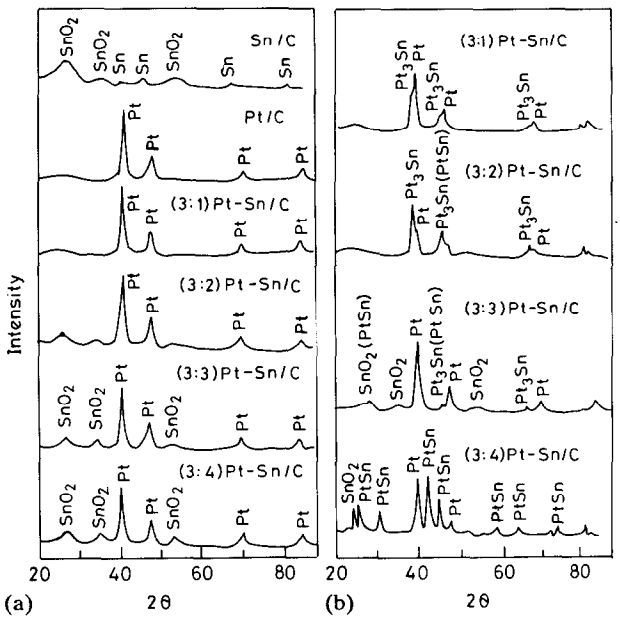

Fig. 6. XRD pattern of Pt–Sn/C catalyst (a) as prepared, and (b) after heating in vacuum at 400 °C for 2 h.

TABLE 1

Distribution of elements in Pt/C and Pt–Sn/C catalysts

Sample	Pt/Sn (molar ratio)	Pt (wt.%)	Sn (wt.%)	C (wt.%)	O (wt.%)	H (wt.%)
Pt/C		16.6		81.19	1.59	0.18
(3:1)Pt–Sn/C	3.0	16.1	3.2	76.76	3.31	0.23
(3:2)Pt–Sn/C	1.55	15.6	6.1	75.78	1.49	0.18
(3:3)Pt–Sn/C	1.0	15.15	9.1	69.22	4.99	0.29
(3:4)Pt–Sn/C	0.75	14.7	11.8	65.36	6.4	0.3
Sn/C			7.2	87.9	3.11	0.27

(3:4)Pt–Sn/C (Fig. 7(c)) catalyst samples. Interestingly, this shift is larger (1.1 eV) for the (3:2)Pt–Sn/C that for (3:4)Pt–Sn/C catalyst (0.4 eV). These shifts can be attributed to the charge transfer from tin to platinum within the catalyst [42, 43]. The larger shift in the maximum absorption for the (3:2)Pt–Sn/C catalyst can also be rationalized from XRD data of the respective catalysts.

The Pt4f XPS of bulk platinum (sample I) is shown in Fig. 8(a). There was a substantial oxygen signal from this sample (the Pt4f:O1s ratio is 7:1), with the result that the Pt4f signal contained an appreciable contribution from a higher binding energy component. The binding energy doublet with $Pt4f_{7/2}$ at 70.8 eV agrees well with the published value (71.1 eV) for platinum metal [44]. By contrast, the binding energy of the $4f_{7/2}$ component of the higher binding energy doublet at 72.1 eV (species 2) is close to the binding energy reported for PtO [44, 45]. The width of the PtO doublet

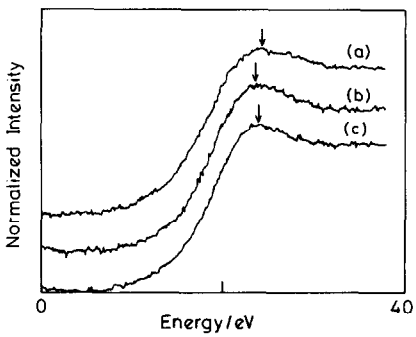

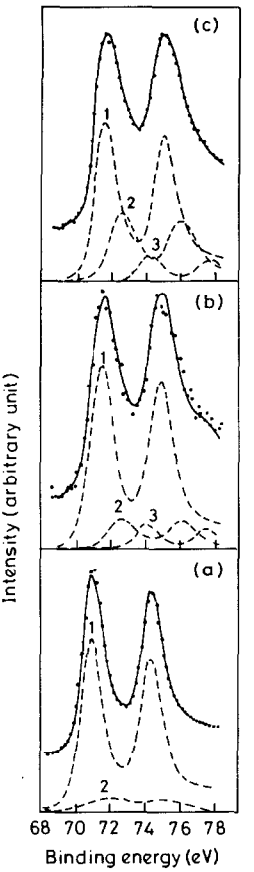

Fig. 7. XANES of (a) Pt/C, (b) (3:2) Pt–Sn/C, and (c) (3:4)Pt–Sn/C catalysts.

Fig. 8. XPS data of Pt4f for: (a) platinum metal (sample I); (b) carbon-supported Pt–Sn catalyst (sample II), and (c) carbon-supported Pt clusters of size 100 Å (sample III). Experimental spectra are shown by dots and fitted spectra by broken lines. Components of least-square-error fit are labelled as 1, 2 and 3.

is appreciably higher than that of the platinum metal signal and its relative intensity is quite low (Table 2). Both of these observations are consistent with the assignment of the higher binding energy doublet to surface-bound PtO.

The Pt4f spectrum of carbon-supported (3:2)Pt–Sn bimetal catalyst (sample II) is given in Fig. 8(b). To achieve a consistent fit of the spectral data, three components were needed, at binding energies 71.3 eV (species 1), 72.2 eV (species 2) and 73.8 eV (species 3). It is noteworthy that the peak position of species 1 is shifted by 0.5 eV towards higher binding energies for sample II in comparison with sample I, whereas the widths of the spectra corresponding to species 1 in Figs. 8(a) and (b) are nearly similar. Also, it is found that species 1 has the highest intensity in both the samples (Table 2). This suggests that species 1 in Fig. 8(b) is also associated with metallic platinum in the Pt–Sn catalyst. The observed shift can arise either from small-cluster-size effects [46] or from charge transfer between platinum and tin in the bimetal. The

TABLE 2

Binding energies and relative intensities of different species in samples I, II and III

Sample	Species	Binding energy of $Pt4f_{7/2}$ (eV)	Relative intensity (%)
I	1	70.8	88
	2	72.1	12
II	1	71.3	74
	2	72.2	17
	3	73.8	9
III	1	71.1	58
	2	72.2	33
	3	73.8	9

peak positions of species 2 and 3 are found to be shifted by 0.9 and 2.5 eV, respectively, to higher binding energies in relation to species 1, and are close to the values of chemical shifts reported for PtO and PtO_2 [44, 45], respectively. It is also observed that the widths of species 2 and 3 are somewhat larger than species 1, while their relative intensities are quite low (Table 2). These observations are consistent with the assignment of species 2 and 3 to a PtO-like and a PtO_2-like surface species, respectively.

In order to understand the nature of the active species in a carbon-supported (3:2)Pt–Sn catalyst sample, a study was made of the XPS of carbon-supported Pt particles of similar size (sample III) as those of the Pt–Sn catalyst. Figure 8(c) shows that the experimental spectra of sample III can be fitted by three components with binding energies 71.1 (1), 72.2 (2) and 73.8 eV (3). Following the arguments similar to those described above for sample II, species 1 is assigned to metallic platinum, and species 2 to PtO-like and species 3 to PtO_2 in supported platinum clusters. It should be noted that the binding energy of the peak due to species 1 is marginally higher in sample II than in sample III, the difference is within experimental error. If there is a charge transfer from tin to platinum sites in the Pt–Sn bimetal, then it is expected that species 1 should have a lower binding energy in this sample than in supported platinum-metal clusters. It could also be conjectured that the shift of 0.4 ± 0.1 eV peak position of the species 1 both in the samples II and III compared with bulk platinum-metal may well arise from a finite-size effect of the supported platinum particles.

It is important to note that the intensity of the PtO signal (species 2) is considerably lower in the supported Pt–Sn catalyst sample than in the supported platinum-particle, while the intensity of the PtO_2 signal (species 3) is relatively unaffected. Thus, it is concluded that the presence of tin in the Pt–Sn bimetal helps in scavenging preferentially PtO impurities from the sample. This removal of oxygen from active platinum sites in the Pt–Sn catalyst enhances its catalytic activity compared with Pt/C, though the platinum particle sizes in both the catalysts are similar. It is noteworthy that during the methanol oxidation, the catalyst is operated in a potential regime in which oxides should not be present but where the supply of active oxygen to the surface is of paramount importance. Both Pt/C and (3:2)Pt–Sn/C catalysts satisfy this condition, but as the latter has more active platinum sites than the former, it should be a more effective catalyst.

The galvanostatic current–potential data for oxidation of methanol on Pt/C and various Pt–Sn/C catalysts electrodes are shown in Fig. 9. The main features of these data are as follows:

(i) The rest potential for Pt–Sn/C catalyst electrodes decreases with increase of tin content in the catalyst and is least for (3:4)Pt–Sn/C that exhibits minimum anodic deviation from the reversible potential.

(ii) Although the anodic deviation of the rest potentials for (3:3)Pt–Sn/C and (3:4)Pt–Sn/C electrodes is less than that for (3:2)Pt–Sn/C, the former two electrodes polarize faster at higher current densities. This is primarily because these electrodes have higher ohmic drops than the (3:2)Pt–Sn/C electrode (see Table 3). The presence of a separate SnO_2 phase within the (3:3)Pt–Sn/C and (3:4)Pt–Sn/C catalysts may also be detrimental to their catalytic activity (see Fig. 6 and Table 1).

(iii) The performance of the (3:2)Pt–Sn/C electrode is better in relation to other catalytic electrodes; it also exhibits the least ohmic drop (see Table 3).

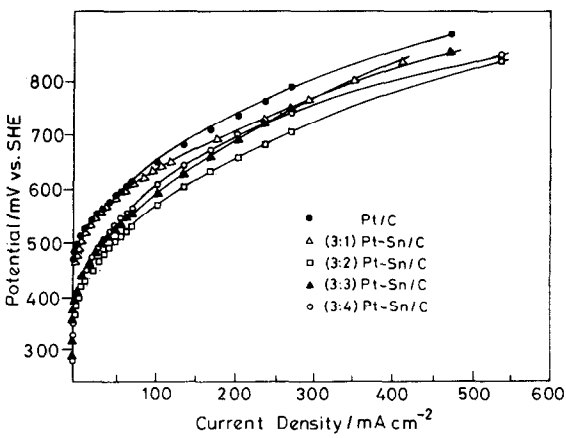

Fig. 9. Galvanostatic-polarization curves for oxidation of methanol in H_2SO_4 at 60 °C on electrodes containing Pt/C, and Pt–Sn/C bimetal catalysts.

TABLE 3

Electrode-kinetic parameters for methanol oxidation in H_2SO_4 on Pt/C and various Pt–Sn/C electrodes

Electrode type	Electrode-kinetic parameters				Ohmic drop		Rest potential vs. SHE (V)
	Tafel data		Graphical data		Experimental (Ω cm^2)	Graphical (Ω cm^2)	
	Slope (mV)	$n\beta$	$(dE/dI)/d(I^{-1})$ (mV)	$n\beta$			
Pt/C	92	0.72	40	0.72	0.50	0.56	0.472
(3:1)Pt–Sn/C	71	0.93	32	0.94	0.67	0.53	0.466
(3:2)Pt–Sn/C	117	0.56	59	0.49	0.42	0.42	0.371
(3:3)Pt–Sn/C	112	0.59	56	0.52	0.51	0.56	0.286
(3:4)Pt–Sn/C	135	0.49	60	0.48	0.44	0.54	0.279

(iv) The observed rest potentials shift more and more towards the reversible value (0.043 V versus SHE) with increasing tin content. This suggests that tin facilitates the chemisorption of methanol.

The current–potential data (corrected both for mass-transfer and ohmic polarizations) indicate distinct Tafel slopes (Fig. 10). To the knowledge of the authors, the data are the first ever to be reported for methanol electrooxidation in sulfuric acid electrolyte. To derive these data, the values of the limiting currents, $i_{l,a}$, have been obtained from digital simulation of current–potential data described elsewhere [47]. The polarization behaviour for (3:2)Pt–Sn/C, (3:3)Pt–Sn/C and (3:4)Pt–Sn/C electrodes is similar, as reflected from the values of the Tafel slopes (see Table 3). It is found that the rate-limiting reaction involves a two-electron process on Pt/C and (3:1)Pt–Sn/C electrodes, but is shifted to a one-electron process on (3:2)Pt–Sn/C, (3:3)Pt–Sn/C and (3:4)Pt–Sn/C electrodes.

The above conjecture is supported by the following analysis of the electrochemical data. The current–potential behaviour of a gas-diffusion electrode under anodic polarization is described in ref. 48, i.e.:

$$E = E_{ocp} - \frac{RT}{n\beta F} \ln \frac{I_{ocp}(I_a - I_{l,a})}{I_a I_{l,a}} + I_a R_u \tag{1}$$

where, E is the observed potential, E_{ocp} the open-circuit potential, I_{ocp} the current density corresponding to E_{ocp}, I_a the observed anodic current, $I_{l,a}$ the anodic-limiting current, β the anodic transfer coefficient, R_u the uncompensated ohmic resistance, F the Faraday constant, R the gas constant, T the temperature, and n the number of electrons. Differentiating eqn. (1) with respect to I_a gives:

$$\frac{dE}{dI_a} = -\frac{RT}{n\beta F} \frac{1}{(I_{l,a} - I_a)} + \frac{RT}{n\beta F} \frac{1}{I_a} + R_u \tag{2}$$

Equating the second derivative of eqn. (2) to zero at the inflection point yields $I_{l,a} = 2I_{inf}$, where I_{inf} is the value of I_a at the inflection point.

If $I_{l,a} \gg I_a$, eqn. (2) transforms to:

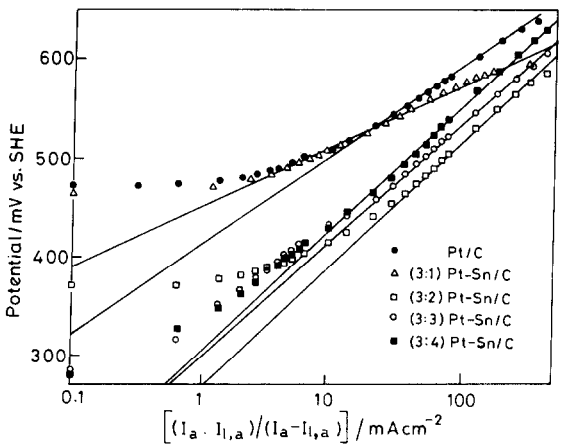

Fig. 10. Polarization curves after correcting data in Fig. 9 for both ohmic and mass-transfer polarizations; full lines indicate Tafel slopes.

$$\frac{dE}{dI_a} = \frac{RT}{n\beta F}\frac{1}{I_a} + R_u \tag{3}$$

The plot of dE/dI_a versus $1/I_a$ leads to a straight line with an intercept R_u and a slope $RT/n\beta F$ that yields directly the value of $n\beta$ for the electrochemical processes on the electrodes. The plots of dE/dI_a versus $1/I_a$ for Pt/C and various Pt–Sn/C electrodes are given in Fig. 11. The R_u and $n\beta$ values derived from these plots are listed in Table 3. An advantage of the present graphical analysis is that it does not require any compensation of the ohmic drop for extracting electrode-kinetic parameters [48]. Furthermore, the polarization component due to mass transfer can be neglected when operating in the range where $I_{l,a} \gg I_a$, as in the present study. The values of $n\beta$ obtained from slopes of these plots, as well as the values of R_u obtained from their intercepts, are close to those obtained experimentally from the Tafel data and the current-interrupter method.

A plausible mechanism to explain methanol oxidation on Pt–Sn/C electrodes, as indicated by the outcomes of this study, is as follows. The first step during methanol oxidation involves a dissociative chemisorption of methanol on the catalyst surface concomitant with successive donation of electrons to the catalyst that makes the chemisorbed species positively charged. The charge transfer from the atomic species to another in the catalyst introduces an extra electrostatic component to the binding energy. This extra component is attractive at the more electronegative species (namely platinum) and is repulsive at the more electropositive species (namely tin) in the bimetal catalyst. A repulsive electrostatic component promotes the separation of the electronic charge trapped at the catalyst surface from the bound protons. Nevertheless,

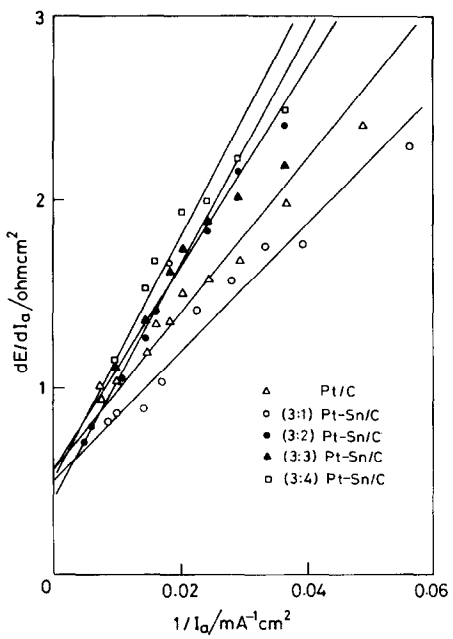

Fig. 11. Plot of dE/dI_a vs. $1/I_a$ obtained from polarization data in Fig. 9; full lines indicate least-squares fit of data (correlation coefficient = 0.98).

the capture of surface protons and carbonaceous COH^- radicals by negatively charged surface atoms will inhibit their desorption.

The subsequent step involves attraction of oxygen species from the aqueous electrolyte to the catalyst surface. This reaction is driven by an electric field across the double layer. At the Pt–Sn catalyst surface, charge transferred from tin to platinum will produce the applied voltage required to attract the oxygen species to the surface at the more electropositive tin atoms. Minimization of the applied voltage required for this step is essential for methanol oxidation. The following step is promoted by the charge transfer from tin to platinum in the catalyst. This alters the adsorbate bond strength as well as the free energy of activation (ΔG_m) for chemical reaction. Therefore, a shift in the onset potential is anticipated with a concomitant change in the exchange current, $i_0 = \exp(-\Delta G_m/RT)$. This was found in the Pt–Sn/C electrodes during the present study. The final rate-determining step involves evolution of CO_2 with regeneration of the catalyst.

In the light of the above discussion, the following scheme is proposed for methanol oxidation on the carbon-supported Pt–Sn electrodes.

$$\begin{array}{l} \mathrm{Sn} \\ | \\ \mathrm{Pt} \end{array} + \mathrm{CH_3OH} \cdots\cdots\cdots\cdots\cdots\rightarrow \begin{array}{l} \mathrm{Sn} \\ | \\ \mathrm{Pt{-}CHO} \end{array} + 3\mathrm{H^+} + 3e^- \quad \text{(step 1)}$$

$$\begin{array}{l} \mathrm{Sn} \\ | \\ \mathrm{Pt{-}CHO} \end{array} + \mathrm{H_2O} \cdots\cdots\cdots\cdots\rightarrow \begin{array}{l} \mathrm{Sn{-}OH} \\ | \\ \mathrm{Pt{-}CHO} \end{array} + \mathrm{H^+} + e^- \quad \text{(step 2)}$$

$$\begin{array}{l} \mathrm{Sn{-}OH} \\ | \\ \mathrm{Pt{-}CHO} \end{array} \cdots\cdots\cdots\cdots\cdots\rightarrow \begin{array}{l} \mathrm{Sn{-}OH} \\ | \\ \mathrm{Pt{-}CO} \end{array} + \mathrm{H^+} + e^- \quad \text{(step 3)}$$

$$\begin{array}{l} \mathrm{Sn{-}OH} \\ | \\ \mathrm{Pt{-}CO} \end{array} \xrightarrow{\text{rate-determining step}} \begin{array}{l} \mathrm{Sn} \\ | \\ \mathrm{Pt} \end{array} + \mathrm{CO_2} + \mathrm{H^+} + e^- \quad \text{(step 4)}$$

Conclusions

Among the various carbon-supported electrodes with varying Pt–Sn compositions, the (3:2)Pt–Sn/C electrodes exhibit the highest catalytic activity towards the electro-oxidation of methanol. The charge transfer from tin to platinum is found to be maximum for the (3:2)Pt–Sn/C catalyst. It is speculated that the charge transfer from tin to platinum within this bimetal catalyst, together with the partial scavenging of oxidic impurities from platinum sites, are the determining factors for the observed synergistic promotion of the methanol oxidation reaction. This is because the catalyst is operated necessarily in a regime in which oxides should not be present but where supply of oxygen to the surface is of paramount importance.

Acknowledgements

The authors thank Professor A. Hamnett, Newcastle, UK, for a critical appraisal of the manuscript. Financial support from the Ministry of Non-conventional Energy Sources, Government of India, New Delhi, is also gratefully acknowledged.

References

1 D.S. Cameron, G.A. Hards, B. Harrison and R.J. Potter, *Platinum Met. Rev., 31* (1987) 173.
2 A. Hamnett and G. Troughton, *Chem. Ind., 3* (1992) 480.
3 B.D. McNicol, *J. Electroanal. Chem., 118* (1981) 71.
4 R. Parsons and T. Vandernoot, *J. Electroanal. Chem., 257* (1987) 9.
5 O. Lindström and A.K. Shukla, *Bull. Electrochem., 7* (1991) 485.
6 S. Juanto, B. Beden, F. Hahn, J.M. Leger and C. Lamy, *J. Electroanal. Chem., 237* (1987) 119.
7 S. Wilhelm, T. Iwasita and W. Vielstich, *J. Electroanal. Chem., 238* (1987) 383.
8 B. Beden, S. Juanto, J.M. Leger and C. Lamy, *J. Electroanal. Chem., 238* (1987) 323.
9 A. Heinzel, R. Holze, C.H. Hamann and J.K. Blum, *Electrochim. Acta, 34* (1989) 657.
10 T. Iwasita, F.C. Nart, B. Lopez and W. Vielstich, *Electrochim. Acta, 37* (1992) 2361.
11 T. Iwasita and F.C. Nart, *J. Electroanal. Chem., 317* (1992) 291.
12 I. Willsau, O. Wolter and J. Heitbaum, *J. Electroanal. Chem., 185* (1985) 163.
13 T. Iwasita, F.C. Nart and W. Vielstich, *Ber. Bunsenges. Phys. Chem., 94* (1990) 1030.
14 K. Kunimatsu, *Ber. Bunsenges. Phys. Chem., 94* (1990) 1025.
15 B. Beden, F. Kadirgan, C. Lamy and J.M. Leger, *J. Electroanal. Chem., 127* (1981) 75.
16 S.A. Campbell and R. Parsons, *J. Chem. Soc., Faraday Trans., 88* (1992) 833.
17 A.N. Haner and P.N. Ross, *J. Phys. Chem., 95* (1991) 3740.
18 M.M.P. Janssen and J. Mollhuysen, *Electrochim. Acta, 21* (1976) 869.
19 A. Aramata, I. Toyoshima and M. Enyo, *Electrochim. Acta, 37* (1992) 1317.
20 G.L. Troughton and A. Hamnett, *Bull. Electrochem., 7* (1991) 488.
21 S. Swathirajan and Y. Mikhial, *J. Electrochem. Soc., 138* (1991) 1321.
22 M. Watanabe, Y. Furuuchi and S. Motoo, *J. Electroanal. Chem., 191* (1985) 367.
23 M.M.P. Janssen and J. Mollhuysen, *Electrochim. Acta, 21* (1976) 861.
24 J.B. Goodenough, A. Hamnett, B.J. Kennedy, R. Manoharan and S.A. Weeks, *Electrochim. Acta, 35* (1990) 199.
25 C.T. Hable and M.S. Wrighton, *Langmuir, 7* (1991) 1305.
26 A. Hamnett and B.J. Kennedy, *Electrochim. Acta, 33* (1988) 1613.
27 S. Swathirajan and Y.M. Mikhail, *J. Electrochem. Soc., 139* (1992) 2105.
28 B.J. Kennedy and A.W. Smith, *J. Electroanal. Chem., 293* (1990) 103.
29 B. Bittins-Cataneo and T. Iwasita, *J. Electroanal. Chem., 238* (1987) 151.
30 A. Hamnett, B.J. Kennedy and F.E. Wagner, *J. Catal., 124* (1990) 30.
31 B.J. Kennedy and A. Hamnett, *J. Electroanal. Chem., 283* (1990) 271.
32 J.B. Goodenough, A. Hamnett, B.J. Kennedy, R. Manoharan and S.A. Weeks, *J. Electroanal. Chem., 240* (1988) 133.
33 S. Wasmus and W. Vielstich, *J. Appl. Electrochem., 23* (1993) 120.
34 S. Hufner and G.K. Wertheim, *Phys. Rev. B, 11* (1975) 678.
35 A.J. Bard and L.R. Faulkner, *Electrochemical Methods: Fundamentals and Applications,* Wiley–Interscience, New York, 1980.
36 A.S. Aricò, V. Antonucci, L. Pino, P.L. Antonucci and N. Giordano, *Carbon, 28* (1990) 598.
37 G.T. Baronetti, S.R. de Miguel, O.A. Scelza, M.A. Fritzler and A.A. Castro, *Appl. Catal., 19* (1985) 77.
38 G. Leitz, H. Leiske, H. Spindler, W. Hanke and J. Volter, *J. Catal., 81* (1983) 17.
39 M. Pourbaix, *Atlas of Electrochemical Equilibria in Aqueous Solutions,* Pergamon, London, 1966.
40 *Powder Diffraction Files (Inorganic Volumes), 35*-1360; *25*-614; *19*-1365; *4*-802; *5*-390; *21*-1250; *33*-1374; JCPDS International Center for Diffraction Data, USA.
41 H.P. Klug and L.E. Alexander, *X-ray Diffraction Procedures for Polycrystalline and Amorphous Materials,* Wiley, New York, 1974.
42 A.N. Manson, J.W. Cook and D.E. Sayers, *J. Phys. Chem., 88* (1984) 2330.
43 J.B. Goodenough, R. Manoharan, A.K. Shukla and K.V. Ramesh, *Chem. Mater., 1* (1989) 391.

44 J.S. Hammond and N. Winograd, *J. Electroanal. Chem., 78* (1977) 55.
45 J. Knecht and G. Stork, *Fresenius' Z. Anal. Chem., 289* (1978) 206.
46 W. Eberhardt, P. Fayet, D.M. Cox, Z. Fu, A. Kaldor, R. Sherwood and D. Sondericker, *Phys. Rev. Lett., 64* (1990) 780.
47 A.S. Aricò, A.K. Shukla, V. Antonucci and N. Giordano, *J. Power Sources, 50* (1994) 177.
48 N. Sugumaran and A.K. Shukla, *J. Power Sources, 39* (1992) 249.